Materials Science in Semiconductor Processing 173 (2024) 108111

Contents lists available at ScienceDirect

Materials Science in Semiconductor Processing

journal homepage: www.elsevier.com/locate/mssp

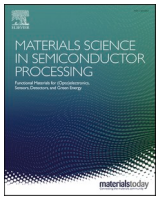

Probing post-growth hydrogen intercalation and H_2 nanobubbles formation in graphene on Ge(110)

L. Persichetti [a,*], D. Paoloni [b,**], A. Apponi [b], L. Camilli [a], A. Caporale [a], V. Babenko [c], S. Hofmann [c], M. Angelucci [d], R. Cimino [d], M. De Seta [b], A. Ruocco [b], L. Di Gaspare [b]

[a] Dipartimento di Fisica, Università di Roma "Tor Vergata", Via Della Ricerca Scientifica, 1 - 00133, Rome, Italy
[b] Dipartimento di Scienze, Università Roma Tre, Viale G. Marconi, 446 - 00146, Rome, Italy
[c] Department of Engineering, University of Cambridge, Cambridge, CB3 0FA, United Kingdom
[d] LNF-INFN, Via E. Fermi 54, 00044, Frascati, Rome, Italy

A B S T R A C T

We investigate the reproducibility of repeated intercalation of hydrogen in graphene/Ge (110) and the formation of H_2 nanobubbles after thermal treatments. By exploiting high-resolution electron energy loss, we obtain direct spectroscopic fingerprints of H_2 trapped gas in the samples when nanobubbles are present and we are able to track the effectiveness of H intercalation via the Ge–H vibrational mode. We correlate the effectiveness of interface re-hydrogenation to the presence of structural defects in graphene as highlighted by Raman spectroscopy. The π-plasmon mode of graphene on Ge (110) is investigated as a function of the hydrogen presence at the interface, revealing that, independent of the hydrogen intercalation status, graphene is weakly interacting on Ge (110).

1. Introduction

The synergistic coupling of graphene (G) with a CMOS compatible substrate could potentially represent a fascinating playground for the development of future electronics [1–4]. Exploiting new graphene-based electronics devices entails the availability of high-quality graphene deposited on large area semiconducting substrates using a mass production compatible technique. In this context, Ge has emerged as a promising candidate for the deposition of graphene by chemical vapor deposition (CVD), due to its catalytic activity on carbon gas precursors and low carbon solubility [5–8]. The most promising results have been obtained on Ge (110) which, contrary to the Ge (100) orientation, remains atomically flat during the growth and promotes epitaxial crystallographic order in graphene [6,9–13]. Extensive studies have been performed also on the interface properties between graphene and Ge (110), with a focus on understanding the complex interplay between Ge surface termination, hydrogen intercalation and electronic and structural properties in graphene, all these factors significantly impacting graphene potential applications in electronic devices [8,14,15]. For example, it has been shown that the thermally induced desorption of hydrogen, which was bonded to Ge surface atoms during the CVD growth, can trigger a transition in Ge surface reconstruction and a modification of the graphene doping [16–21]. This offers opportunities for tailoring the electronic characteristics of graphene for specific device applications. Moreover, the de-intercalation of hydrogen in the graphene/Ge system has been associated with the formation of hydrogen nanobubbles at the interface [22,23]. These nanobubbles, comprised of trapped hydrogen gas, can have a profound impact on the mechanical and electronic properties of graphene, due to a local modification of strain status. For instance, the strain engineering strategy via the formation of nanobubbles has been proposed for generating pseudo-magnetic fields in graphene [24,25].

Up to now, hydrogen nanobubble formation and, more in general, the intercalation/de-intercalation of hydrogen in G/Ge (110) have been studied morphologically and spectroscopically by looking at the changes in the Ge surface reconstruction as well as in the core level line shapes by using X-ray photoelectron spectroscopy (XPS) [22,23]. In this work, we investigate the interface properties of graphene on Ge (110), with a specific focus on the reproducibility of repeated intercalation of hydrogen and the formation of hydrogen nanobubbles. By using high-resolution electron energy loss spectroscopy (HR-EELS) we directly probe the presence of the Ge–H bond in the H-intercalated G/Ge (110) samples as well as the presence of H_2 gas trapped underneath graphene, after thermal treatments leading to the formation of nanobubbles. By combining spectroscopy and microscopy techniques, we elucidate the intriguing interplay among Ge surface reconstruction, easiness of

* Corresponding author.
** Corresponding author.
E-mail addresses: luca.persichetti@uniroma2.it (L. Persichetti), daniele.paoloni@uniroma3.it (D. Paoloni).

https://doi.org/10.1016/j.mssp.2024.108111
Received 6 December 2023; Accepted 3 January 2024

Table 1
Summary of the samples described in the results section and their main features.

Sample	Description	Status of the G/Ge (110) interface	Post-growth treatments
S_H	As-grown pristine sample.	Intercalated by H passivating the Ge surface.	Transferred in air after growth and outgassed in UHV to 100 °C before STM measurements.
S_{DH}	Sample obtained by UHV annealing to 650 °C of S_H.	Hydrogen de-intercalated.	After deintercalation exposed to air for Raman measurements and STM. Outgassed for 10 min to 420 °C in UHV prior to XPS measurements.
S_{RH}	Sample obtained by exposing S_{DH} to H_2 ($p = 6 \times 10^{-8}$ mbar) for 40 min at 650 °C.	Hydrogen re-intercalated.	All the characterization were performed in UHV.
$S_{(DH)x2}$	Sample obtained by annealing S_{RH} to 370 °C in UHV.	H_2 nanobubbles.	All the characterization were performed in UHV.
S_{LEED}	Sample obtained by prolonged exposure of $S_{(DH)x2}$ to low energy electrons of *c*-LEED measurements.	Hydrogen de-intercalated without nanobubbles.	All the characterization were performed in UHV.
S_{anneal}	Sample obtained by annealing S_{LEED} in UHV (up to 450 °C) and then exposing to H_2 at 670 °C (procedure repeated 3 times).	Hydrogen de-intercalated.	Exposed to air for Raman measurement.

hydrogen intercalation and structural quality of graphene.

Our findings hold promise for advancing the fundamental understanding of graphene-substrate interactions and for guiding the design of novel graphene-based devices with tailored electronic properties and enhanced functionality.

2. Materials and methods

Single layer graphene was deposited on Ge (110) substrates (purchased by g-materials, Germany) by chemical vapor deposition in a tube furnace using methane, hydrogen and argon as carrier gas. Deposition temperature was T = 930 °C. Following the growth step, methane was removed from the deposition chamber and samples were cooled in H_2–Ar atmosphere. Further details about the deposition are provided in Ref. [23]. These growth conditions produce single layer graphene with H atoms intercalated at the G/Ge interface [9,23].

Samples were characterized by using Raman spectroscopy, XPS, HR-EELS, scanning angle low-energy electron diffraction (SA-LEED) and scanning tunneling microscopy (STM).

Raman measurements were performed in air by using a Renishaw Raman InVia Reflex μ–spectrometer equipped with a diode laser at 532 nm, operating at a nominal output power of 100 mW, and with a Leica DM2700 M confocal microscope. The spectra were recorded by using the 100 × objective, with a nominal spectral resolution of about 1 cm^{-1}. The intensity ratios of the Raman bands were calculated using the integrated area of the peaks.

SA-LEED measurements were carried out using a monochromatic electron gun and a hemispherical electron analyzer. The primary energy E_p is equal to 72 eV. Reciprocal space is spanned by changing the momentum transfer **q** of the diffraction experiment. In the specular (elastic) conditions, the component of **q** parallel to the surface ($\mathbf{q}_{//}$) vanishes, defining the zero-th order diffraction peak. By scanning the polar angle θ (while keeping fixed the incidence and collection angles), $\mathbf{q}_{//}$ is changed and a surface diffraction peak is observed for $\mathbf{q}_{//}$ matching a surface reciprocal lattice vector **G**. SA-LEED pattern explores a singular reciprocal space direction, and the other directions can be examined by rotating the sample azimuthally (φ angle). More details on the experimental setup and geometry can be found in Ref. [26]. SA-LEED measurements were paralleled by conventional back-display LEED (*c*-LEED).

XPS measurements were carried out by using a monochromatized Al $K_{\alpha 1}$ source and a hemispherical analyzer equipped with a multichannel detector. The total resolution of the apparatus is 0.45 eV. The energy calibration was established by comparing the measured binding energy of the graphite C 1s peak with the literature value (equal to 284.5 eV [27]). All XPS spectra were deconvoluted with Voigt profiles but the sp^2 component in C 1s spectra reproduced with a Doniach-Sunjic lineshape.

EELS experiments were performed using the same electron gun used for SA-LEED, operating at E_p = 91 eV and the same hemispherical analyzer employed for the XPS measurements. The angle between the source and analyzer is 120° and the measurements were acquired in specular reflection geometry. The peaks are deconvoluted using Voigt profiles. The energy resolution of about 60 meV of this technique allows to investigate vibrational modes of the sample [28].

A pulse-tube-cooler based low-temperature (T < 10 K) STM (Infinity system, Scienta Omicron GmbH, Germany) operating in UHV and working in constant current mode with W tips was employed for the investigation of the sample morphology. STM images were analyzed using the Gwyddion software.

In Table 1, we summarize the samples described in the Results section and their main features.

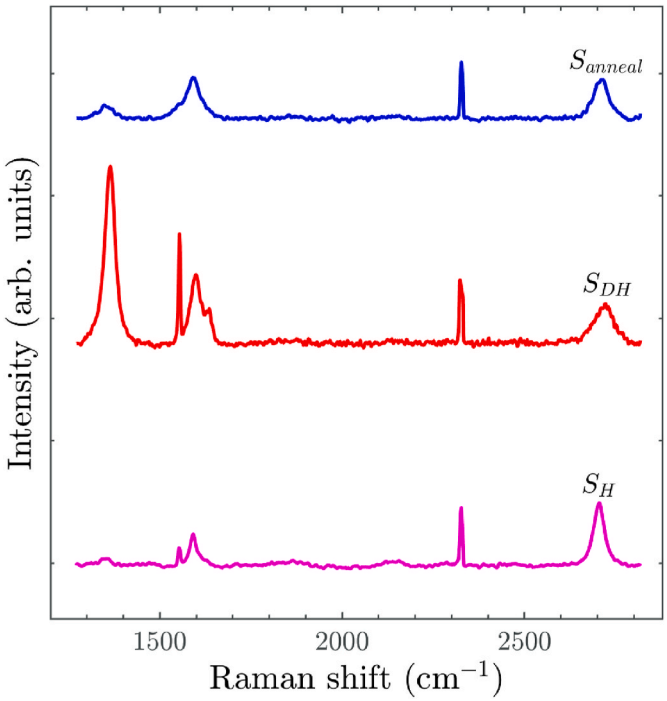

Fig. 1. Raman spectra of the G/Ge (110) samples showing the graphene 2D (around 2720 cm^{-1}), G (around 1590 cm^{-1}), D' (around 1634 cm^{-1}) and D (around 1360 cm^{-1}) bands. Lowest magenta curve: as grown hydrogen intercalated sample (S_H); middle red curve: sample after the first post-growth dehydrogenation of the G/Ge (110) interface (S_{DH}); top blue curve: sample after multiple cycles of exposure to H_2 and UHV annealing (S_{anneal}). The data points are extracted from Raman spatial maps. Spectra are normalized to the N_2 peak observed around 2326 cm^{-1}.

3. Results

We investigate post-growth de-intercalation and the subsequent re-intercalation of hydrogen in G/Ge (110) samples. First, we characterize the pristine sample S_H with H atoms intercalated at the G/Ge interface (See Table 1) using the growth conditions outlined in the previous section. Its Raman spectrum, shown in Fig. 1 (lowest curve), is characterized by a sharp 2D band well fitted by a single Lorentzian peak with a full-width-at-half-maximum Γ_{2D} of 35 cm^{-1}, a 2D/G peak ratio of about 3, as expected for monolayer graphene on germanium [14,15,29], and a negligible D peak due to defects.

A STM image of the pristine hydrogen-intercalated sample S_H is reported in Fig. 2(a). The graphene lattice is clearly visible, while the Ge surface atom arrangement is hindered by the decoupling hydrogen layer [19,21].

By performing a UHV annealing to 650 °C of sample S_H, we obtain the hydrogen de-intercalated sample S_{DH}, whose Raman spectrum is reported in Fig. 1 (middle curve). The dehydrogenation of the interface results in the halving of the 2D/G peak ratio and in the increase of the Γ_{2D} of about 47 %. Besides, we observe a drastic increase in the D peak amplitude and the rise of the D' peak. All these features indicate a worsening of the crystalline quality of graphene with the introduction of a large amount of defects following the breaking of the Ge–H bonds and the escaping of hydrogen from the interface promoted by thermal annealing. As shown in Fig. 2 (b), the STM image of the sample S_{DH} with de-hydrogenated interface reveals the coexistence of regions with a (6 × 2) reconstruction and regions where atomic rows typical of the (1 × 1)-reconstruction are observed. As known in literature, the presence of these two reconstructions is peculiar to the Ge (110) surface underneath the graphene layer when the intercalated hydrogen is thermally removed from the interface, the relative amount of the two phases depending on the temperature of the thermal process employed [16–19,21,23].

After the *ex-situ* Raman and STM characterizations, the S_{DH} sample has been re-introduced in UHV for the re-hydrogenation of the interface. In Fig. 3(a) and (b), we report the C 1s and Ge $2p_{3/2}$ core level XPS spectra acquired before (S_{DH}) and after (S_{RH}) the hydrogen re-intercalation performed using H_2 (see Table 1 for details). In the S_{DH} sample, two components at higher binding energy with respect to the main Ge $2p_{3/2}$ peak are visible, corresponding to GeO (blue curve) and GeO_2 (green curve) oxides [30]. The presence of residual oxides components can be explained by the fact that the sample has been exposed to air during *ex-situ* characterizations before the XPS. Since the atomic structure of the Ge surface is clearly visible in the STM images of sample S_{DH} after air exposure [Fig. 1(b)], we attribute the presence of the small Ge oxides components in the XPS spectrum to local oxidation at the defect sites of the graphene layer and regions of the substrate not covered by graphene (estimated to be <5 % from XPS) [31]. This is in agreement with the well know property of graphene monolayer to preserve the Ge surface from oxidation [32–35]. As for the C 1s spectrum of S_{DH}, we find a main asymmetric peak centered around 284.4 eV due to graphene, well fitted by a Doniach-Sunjic lineshape with a minor component at higher binding energy attributed to *C*–OH bond due to adventitious contamination [36].

Significant changes occur in the XPS spectra after annealing in H_2 atmosphere (sample S_{RH}), as shown by the top spectra in Fig. 3(a) and (b). Only a negligible GeO component is detected in the Ge $2p_{3/2}$ spectrum, showing the effectiveness of the adopted procedure to remove the residual oxide from the Ge surface. Also, in the C 1s spectrum, the contribution from contaminants is now negligible and a narrower graphene sp^2 peak is found.

In order to prove the H presence at the interface and the effectiveness of the re-intercalation procedure, we performed HR-EELS spectroscopy of the samples. Data relative to energy loss up to 1.8 eV, where the peaks due to Ge–H and H–H vibration modes should appear, are shown in Fig. 4.

In the S_{DH} spectrum, no peaks are observable, confirming the absence of hydrogen at the G/Ge (110) interface and thus its de-hydrogenation. Conversely, the spectrum of the S_{RH} sample features a peak at 0.21 eV, associated with vibrational stretching modes involving hydrogen and germanium (Ge–H) [37]. This finding indicates that hydrogen has been effectively re-intercalated below graphene, thus directly proving the effectiveness of the re-intercalation procedure.

The EELS of this S_{RH} sample in a wider energy range, including the graphene π-plasmon mode, is displayed in Fig. 5. Two peaks are clearly visible, well reproduced by a fit with two Gaussian components located at 5.7 eV and 8.5 eV. The higher energy peak is due to surface-related transitions of Ge [38,39]. Conversely, the peak at 5.7 eV is due to the graphene π-plasmon [40–43]. In our experimental conditions, this peak is clearly visible, and its energy position therefore easily determined. The obtained value is very close to that obtained in the same setup and conditions for free-standing graphene on a grid, i.e. 5.9 eV [43] and, therefore, indicates a weakly interacting graphene [44–46] with the Ge (110) substrate. Notice that we do not observe a significant energy shift of the π-plasmon between hydrogen intercalated and de-intercalated samples (See supplementary information), suggesting that the presence of hydrogen at the interface plays a minor role in determining the interaction with the Ge substrate. This result is in agreement with Ref. [47], where a weakly-interacting graphene was reported for a G/Ge (110) sample deposited without hydrogen.

We also investigated the crystalline quality of the S_{RH} sample by using SA-LEED. We explored two azimuthal orientations, corresponding to the Γ-M (φ = 0°) and the Γ-K (φ = 30°) directions, as shown in Fig. 6. In each spectrum, both the Γ-M and Γ-K peaks are present. This evidences the presence of two graphene crystalline domains rotated by 30°, as typically observed for G/Ge (110) [10,47]. We can estimate the relative coverage of these two domains by the intensity of the four diffraction peaks measured in the two azimuthal directions. This calculation reveals that the fraction coverage of the larger domain is about 85 % [48].

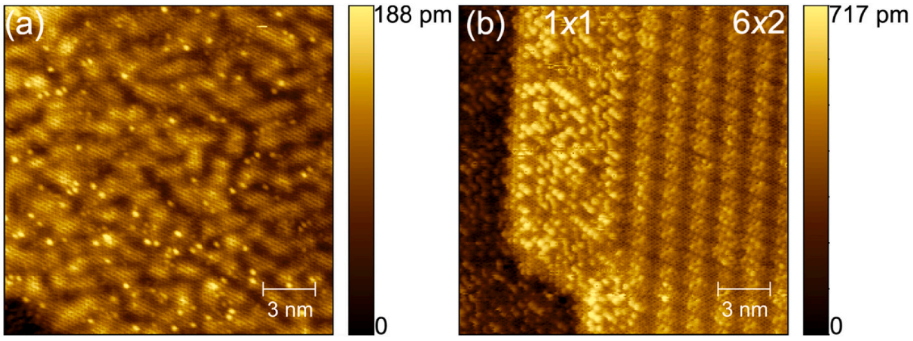

Fig. 2. Low-temperature (T = 9 K) STM images of (a) the as-grown hydrogen-intercalated S_H sample and (b) the S_{DH} sample with de-hydrogenated interface. In the latter the (1 × 1) and (6 × 2) reconstructions of the Ge (110) surface underneath graphene are visible.

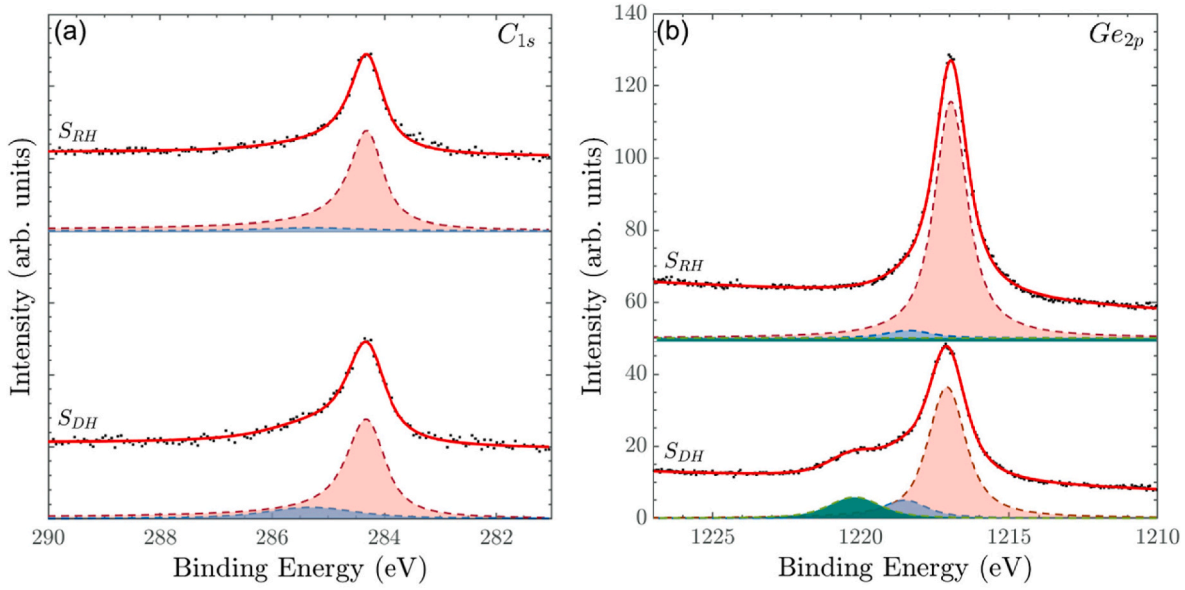

Fig. 3. XPS spectra of the (a) C 1s and (b) Ge $2p_{3/2}$ peaks of S_{DH} and S_{RH} samples. Experimental datapoints are shown as dots; continuous red lines are the fits to the data. The main fitting components for C 1s and Ge $2p_{3/2}$ are represented by the red shaded areas. For C 1s, the blue component is due to *C*–OH. For Ge $2p_{3/2}$, the blue and green shaded areas are attributed to GeO and GeO_2, respectively.

Then, we investigated by HR-EELS the effect of further annealing on the H intercalated sample S_{RH}. We first annealed the S_{RH} sample to 370 °C in UHV to desorb H [49]. As indicated in Table 1, we refer to this sample as $S_{(DH)x2}$. The corresponding HR-EELS spectrum is shown in Fig. 4 (third curve from the bottom). In this spectrum, the GeH component at 0.21 eV is no more present and we observe the rise of a new peak at 0.55 eV. The latter is attributed to a vibrational mode of the H_2 molecule [50]. The presence of this peak is compatible with the formation of H_2 nanobubbles between the graphene layer and the germanium surface, resulting from the breaking of the bond between germanium and hydrogen during the annealing at 370 °C. An example of a nanobubble detected by STM on the sample surface is shown as an inset in Fig. 4. These bubbles that trapped H_2 molecules before the complete removal of hydrogen from the interface have been observed by STM in the same system [22] and experimental conditions [23]. The fact that after the H desorption from the Ge surface the H_2 gas remains trapped in the bubbles between the Ge surface and graphene suggests that graphene defects able to provide the escape route for the gas have been at least partially healed in the thermal processes performed on the sample (H_2 exposure at 670 °C and annealing to 370 °C). We noticed that these H_2 nanobubbles are very sensitive to the exposure to electrons of low energy, their EELS signature disappearing after the *c*-LEED measurements performed using high electron current, of the order of μA (topmost curve in Fig. 4, S_{LEED}), or thermal treatment above 600 °C [23].

Finally, to confirm that the presence of defects in the graphene layer is necessary to re-intercalate H on the G/Ge (110) interface, we repeated the H_2 exposure on a graphene layer without defects. Knowing that the defects in graphene on Ge (110) produced by the H de-intercalation can be healed by thermal treatments [23], we thus annealed the S_{LEED} sample in UHV (up to 450 °C) and then we expose it to H_2 at 670 °C, repeating this procedure three times (See Table 1). After each cycle, we performed HR-EELS and XPS measurements. We did not detect any significant change in the XPS and HR-EELS spectra. This indicates that the G/Ge (110) interface remains in the dehydrogenated status, and thus no further H re-intercalation can be obtained. The Raman spectrum acquired at the end of this treatment cycle is shown in Fig. 1 (topmost curve, sample S_{anneal}). It can be noticed that effectively the Raman features due to defects (D and D' peaks) are almost absent. Also in terms of the 2D/G intensity ratio, the quality of graphene is significantly improved with respect to the S_{DH} sample, confirming the effectiveness of thermal annealing in the restoring of graphene quality.

To summarize, our data demonstrated that H_2 gas can be formed and locally trapped in bubbles at the interface between G and Ge (110). Such nanobubble formation in CVD hydrogen-intercalated graphene/Ge (110) samples had been up to now obtained by a local electrical stimulus via an AFM tip [22] or thermal treatments [23]. In both the cases, the presence of trapped H_2 gas molecules in the nanobubbles was argued without a direct fingerprint. Here, we showed such direct evidence by detecting the H–H vibrational mode in the samples with the nanobubbles by using HR-EELS. We also found that the complete hydrogen removal from the interface results in a very defective graphene with respect to the as-grown sample, as Raman shows. It is reasonable to assume that the formation of these defects is produced by H_2 gas escaping from the bubbles, since Raman worsens as the annealing temperature is increased up to the disappearance of the bubbles [23]. Starting from this defective graphene, we found that hydrogen re-intercalation can be easily obtained by exposing the sample to molecular hydrogen at 650 °C. We thus believe that the defects in the graphene layer are the way for H_2 to overcome the graphene barrier, reaching the Ge surface underneath. Conversely, we found that, when defects are healed by thermal treatments, the re-intercalation of hydrogen is ineffective.

We also detected a direct fingerprint of hydrogen re-intercalation, which was hinted up to now by changes in the Ge surface reconstruction detected by STM [17], by observing the Ge–H mode in EELS. Interestingly, independent of the passivation of the Ge surface by hydrogen, we find that graphene is free-standing on Ge (110), as shown by the energy of the π-plasmon mode, in agreement with the results reported in Ref. [47] where graphene was deposited without hydrogen.

In conclusion, we investigated the properties of the G/Ge (110) interface following thermal treatments in H_2 and UHV, obtaining hydrogen de-intercalation resulting in H_2 nanobubble formation. The introduction of nanobubbles in graphene had been proposed as a possible route for strain engineering of graphene and control over its electronic properties [24,25]. We evidenced that the possibility to obtain hydrogen re-intercalation is correlated to the presence of defects in graphene. Our study thus provides useful information for developing control over the G/Ge interface and, in general, for growth recipes aiming at the controllable synthesis of 2D materials.

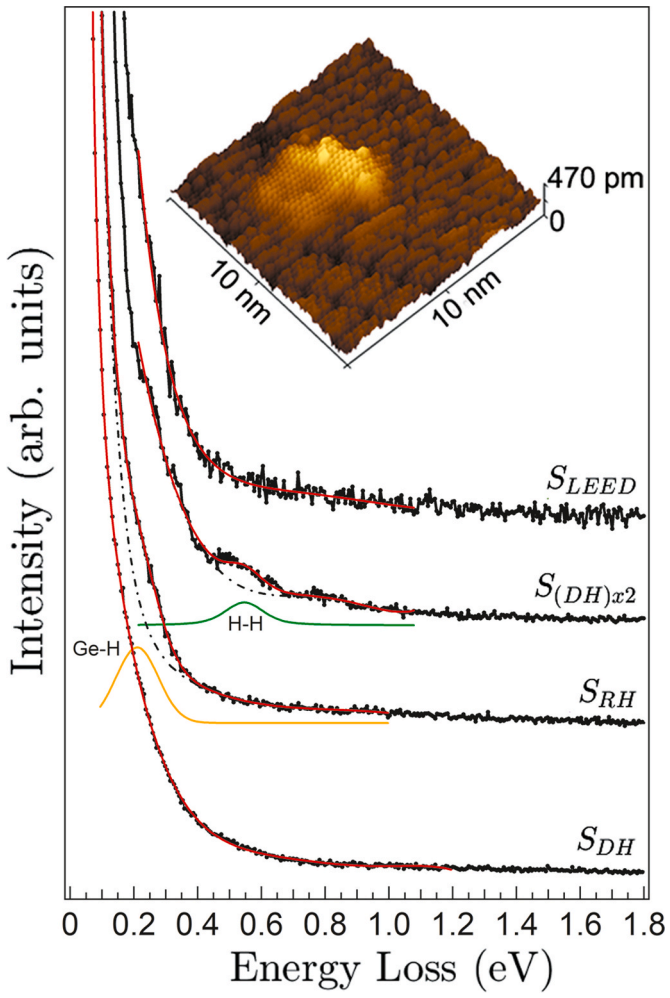

Fig. 4. HR-EELS spectra up to 1.8 eV losses for the different samples described in text. We evidenced the component due vibrational modes involving hydrogen and germanium Ge–H (orange curve in S_{RH}), and the component due the vibrational mode of H_2 molecule, H–H (green curve in S_{DHx2}). To describe the tail of the elastic peak, we use a decreasing exponential plus a third-degree polynomial, represented as the black dashed-dotted curve. The red continuous line if the total fit of the experiment data. In the inset, we report an STM image at 9 K of a H_2 nanobubble below graphene.

CRediT authorship contribution statement

L. Persichetti: Conceptualization, Funding acquisition, Investigation, Writing – original draft. **D. Paoloni:** Formal analysis, Investigation, Writing – review & editing. **A. Apponi:** Investigation, Writing – review & editing. **L. Camilli:** Methodology, Writing – review & editing. **A. Caporale:** Investigation. **V. Babenko:** Investigation. **S. Hofmann:** Funding acquisition, Methodology, Writing – review & editing. **M. Angelucci:** Methodology. **R. Cimino:** Methodology. **M. De Seta:** Conceptualization, Writing – original draft. **A. Ruocco:** Conceptualization, Supervision, Writing – review & editing. **L. Di Gaspare:** Conceptualization, Supervision, Writing – original draft.

Declaration of generative AI and AI-assisted technologies

During the preparation of this work D.Paoloni used openAI/chatGPT in order to improve readability and language. After using this tool, the author reviewed and edited the content as needed and takes full responsibility for the content of the publication.

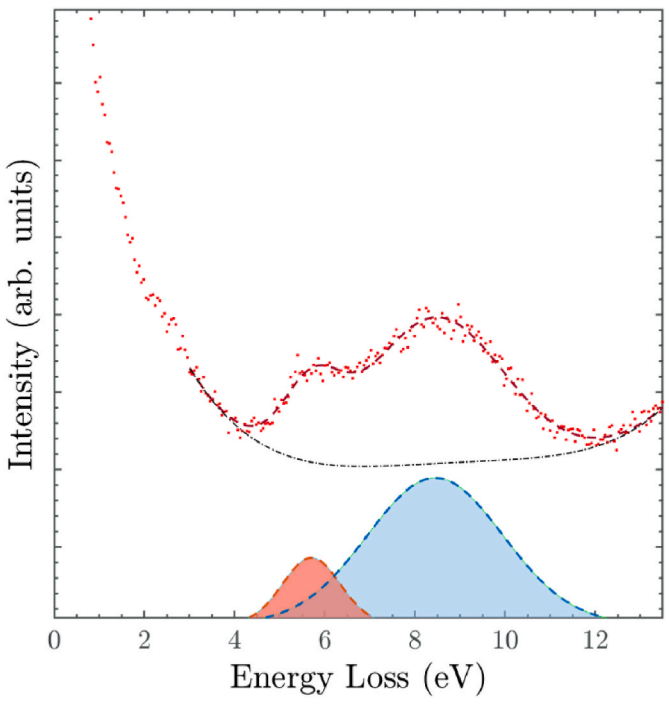

Fig. 5. EELS spectra of the S_{RH} sample in a wide energy range where the Ge surface-related transition (cyan component) and the π-plasmon of graphene (red component) are observed. The dotted-dashed black curve is the spectrum background.

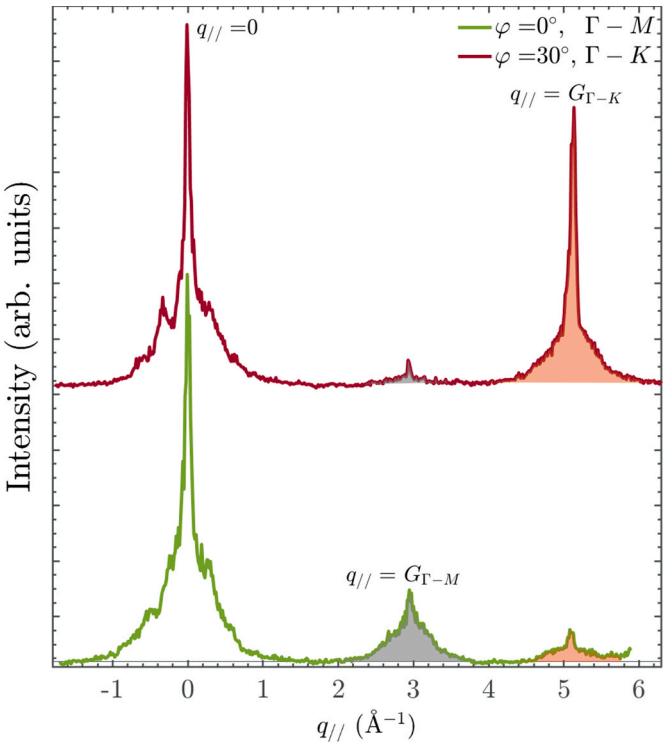

Fig. 6. SA-LEED spectra of the S_{RH} sample acquired along the Γ-M (green) and Γ-K (red) directions. The specular reflection is observed for $q// = 0$. Diffraction peaks appear when $q//$ matches a reciprocal lattice vector of the surface, **G**.

Declaration of competing interest

The authors declare that they have no known competing financial interests or personal relationships that could have appeared to influence the work reported in this paper.

Data availability

The data that has been used is confidential.

Acknowledgements

This work was supported by The Italian Ministry for Universities and Research (MUR) under the Grant of Excellence Departments, (ARTICOLO 1, COMMI 314–337 LEGGE 232/2016) to Department of Science, Roma Tre University. We acknowledge support from Lazio Innova (Regione Lazio, Italy) through the project "Gruppi di ricerca 2020" A0375-2020-36566.

S.H. and V.B. acknowledge funding from EPSRC (EP/T001038/1, EP/P005152/1).

Appendix A. Supplementary data

Supplementary data to this article can be found online at https://doi.org/10.1016/j.mssp.2024.108111.

References

[1] K.S. Novoselov, V.I. Fal'ko, L. Colombo, P.R. Gellert, M.G. Schwab, K. Kim, A roadmap for graphene, Nature 490 (2012) 192.
[2] J.-H. Lee, S.-G. Kang, H.-S. Jang, J.-Y. Moon, D. Whang, Graphene on group-IV elementary semiconductors: the direct growth approach and its applications, Adv. Mater. (2019) 1803469.
[3] D. Akinwande, C. Huyghebaert, C.-H. Wang, M.I. Serna, S. Goossens, L.-J. Li, H.S. P. Wong, F.H.L. Koppens, Graphene and two-dimensional materials for silicon technology, Nature 573 (2019) 507–518.
[4] D. Neumaier, S. Pindl, M.C. Lemme, Integrating graphene into semiconductor fabrication lines, Nat. Mater. 18 (2019) 525–529.
[5] G. Wang, M. Zhang, Y. Zhu, G. Ding, D. Jiang, Q. Guo, S. Liu, X. Xie, P.K. Chu, Z. Di, X. Wang, Direct growth of graphene film on germanium substrate, Sci. Rep. 3 (2013) 2465.
[6] B. Kiraly, R.M. Jacobberger, A.J. Mannix, G.P. Campbell, M.J. Bedzyk, M.S. Arnold, M.C. Hersam, N.P. Guisinger, Electronic and mechanical properties of graphene–germanium interfaces grown by chemical vapor deposition, Nano Lett. 15 (2015) 7414–7420.
[7] A.M. Scaparro, V. Miseikis, C. Coletti, A. Notargiacomo, M. Pea, M. De Seta, L. Di Gaspare, Investigating the CVD synthesis of graphene on Ge(100): toward layer-by-layer growth, ACS Appl. Mater. Interfaces 8 (2016) 33083–33090.
[8] I. Pasternak, P. Dabrowski, P. Ciepielewski, V. Kolkovsky, Z. Klusek, J. M. Baranowski, W. Strupinski, Large-area high-quality graphene on Ge(001)/Si (001) substrates, Nanoscale 8 (2016) 11241–11247.
[9] J.-H. Lee, E.K. Lee, W.-J. Joo, Y. Jang, B.-S. Kim, J.Y. Lim, S.-H. Choi, S.J. Ahn, J. R. Ahn, M.-H. Park, C.-W. Yang, B.L. Choi, S.-W. Hwang, D. Whang, Wafer-Scale growth of single-crystal monolayer graphene on reusable hydrogen-terminated germanium, Science 344 (2014) 286–289.
[10] L. Persichetti, M. De Seta, A.M. Scaparro, V. Miseikis, A. Notargiacomo, A. Ruocco, A. Sgarlata, M. Fanfoni, F. Fabbri, C. Coletti, L. Di Gaspare, Driving with temperature the synthesis of graphene on Ge(110), Appl. Surf. Sci. 499 (2020) 143923.
[11] J. Tesch, F. Paschke, M. Fonin, M. Wietstruk, S. Böttcher, R.J. Koch, A. Bostwick, C. Jozwiak, E. Rotenberg, A. Makarova, B. Paulus, E. Voloshina, Y. Dedkov, The graphene/n-Ge(110) interface: structure, doping, and electronic properties, Nanoscale 10 (2018) 6088–6098.
[12] L. Di Gaspare, A.M. Scaparro, M. Fanfoni, L. Fazi, A. Sgarlata, A. Notargiacomo, V. Miseikis, C. Coletti, M. De Seta, Early stage of CVD graphene synthesis on Ge (001) substrate, Carbon 134 (2018) 183–188.
[13] M. Lukosius, J. Dabrowski, J. Kitzmann, O. Fursenko, F. Akhtar, M. Lisker, G. Lippert, S. Schulze, Y. Yamamoto, M.A. Schubert, H.M. Krause, A. Wolff, A. Mai, T. Schroeder, G. Lupina, Metal-free CVD graphene synthesis on 200 mm Ge/Si (001) substrates, ACS Appl. Mater. Interfaces 8 (2016) 33786–33793.
[14] F. Akhtar, J. Dabrowski, R. Lukose, C. Wenger, M. Lukosius, Chemical vapor deposition growth of graphene on 200 mm Ge(110)/Si wafers and ab initio analysis of differences in growth mechanisms on Ge(110) and Ge(001), ACS Appl. Mater. Interfaces 15 (2023) 36966–36974.
[15] T. Wang, P. Li, X. Hu, M. Gao, Z. Di, Z. Xue, M. Zhang, Wafer-scale fabrication of single-crystal graphene on Ge(110) substrate by optimized CH4/H2 ratio, Appl. Surf. Sci. 529 (2020) 147066.
[16] H.W. Kim, W. Ko, W.-J. Joo, Y. Cho, Y. Oh, J. Ku, I. Jeon, S. Park, S.W. Hwang, Unraveling the structural and electronic properties of graphene/Ge(110), J. Phys. Chem. Lett. 9 (2018) 7059–7063.
[17] D. Zhou, Z. Niu, T. Niu, Surface reconstruction of germanium: hydrogen intercalation and graphene protection, J. Phys. Chem. C 122 (2018) 21874–21882.
[18] G.P. Campbell, B. Kiraly, R.M. Jacobberger, A.J. Mannix, M.S. Arnold, M. C. Hersam, N.P. Guisinger, M.J. Bedzyk, Epitaxial graphene-encapsulated surface reconstruction of Ge(110), Phys. Rev. Mater. 2 (2018) 044004.
[19] B. Kiraly, A.J. Mannix, R.M. Jacobberger, B.L. Fisher, M.S. Arnold, M.C. Hersam, N. P. Guisinger, Driving chemical interactions at graphene-germanium van der Waals interfaces via thermal annealing, Appl. Phys. Lett. 113 (2018) 213103.
[20] S.J. Ahn, H.W. Kim, I.B. Khadka, K.B. Rai, J.R. Ahn, J.-H. Lee, S.G. Kang, D. Whang, Electronic structure of graphene grown on a hydrogen-terminated Ge (110) wafer, J. Kor. Phys. Soc. 73 (2018) 656–660.
[21] M. Galbiati, L. Persichetti, P. Gori, O. Pulci, M. Bianchi, L. Di Gaspare, J. Tersoff, C. Coletti, P. Hofmann, M. De Seta, L. Camilli, Tuning the doping of epitaxial graphene on a conventional semiconductor via substrate surface reconstruction, J. Phys. Chem. Lett. 12 (2021) 1262–1267.
[22] P. Jia, W. Chen, J. Qiao, M. Zhang, X. Zheng, Z. Xue, R. Liang, C. Tian, L. He, Z. Di, X. Wang, Programmable graphene nanobubbles with three-fold symmetric pseudo-magnetic fields, Nat. Commun. 10 (2019) 3127.
[23] L. Camilli, M. Galbiati, L. Di Gaspare, M. De Seta, I. Pís, F. Bondino, A. Caporale, V. P. Veigang-Radulescu, V. Babenko, S. Hofmann, A. Sodo, R. Gunnella, L. Persichetti, Tracking interfacial changes of graphene/Ge(110) during in-vacuum annealing, Appl. Surf. Sci. 602 (2022), 154291-154291.
[24] N. Levy, S.A. Burke, K.L. Meaker, M. Panlasigui, A. Zettl, F. Guinea, A.H.C. Neto, M. F. Crommie, Strain-induced pseudo–magnetic fields greater than 300 tesla in graphene nanobubbles, Science 329 (2010) 544–547.
[25] E. Khestanova, F. Guinea, L. Fumagalli, A.K. Geim, I.V. Grigorieva, Universal shape and pressure inside bubbles appearing in van der Waals heterostructures, Nat. Commun. 7 (2016) 12587.
[26] D. Paoloni, A. Ruocco, Cu-phthalocyanine long-range ordered bulk growth due to the weak interaction with highly oriented pyrolytic graphite substrate, Surf. Sci. 735 (2023) 122322.
[27] K.L. Smith, K.M. Black, Characterization of the treated surfaces of silicon alloyed pyrolytic carbon and SiC, J. Vac. Sci. Technol. A 2 (1984) 744–747.
[28] G. Di Filippo, A. Liscio, A. Ruocco, The evolution of hydrogen induced defects and the restoration of π-plasmon as a monitor of the thermal reduction of graphene oxide, Appl. Surf. Sci. 512 (2020) 145605.
[29] L. Persichetti, L. Di Gaspare, F. Fabbri, A.M. Scaparro, A. Notargiacomo, A. Sgarlata, M. Fanfoni, V. Miseikis, C. Coletti, M. De Seta, Abrupt changes in the graphene on Ge(001) system at the onset of surface melting, Carbon 145 (2019) 345–351.
[30] N.A. Tabet, M.A. Salim, A.L. Al-Oteibi, XPS study of the growth kinetics of thin films obtained by thermal oxidation of germanium substrates, J. Electron. Spectrosc. Relat. Phenom. 101–103 (1999) 233–238.
[31] R.M. Jacobberger, M.J. Dodd, M. Zamiri, A.J. Way, M.S. Arnold, M.G. Lagally, Passivation of germanium by graphene for stable graphene/germanium heterostructure devices, ACS Appl. Nano Mater. 2 (2019) 4313–4322.
[32] F. Cavallo, R. Rojas Delgado, M.M. Kelly, J.R. Sánchez Pérez, D.P. Schroeder, H. G. Xing, M.A. Eriksson, M.G. Lagally, Exceptional charge transport properties of graphene on germanium, ACS Nano 8 (2014) 10237–10245.
[33] R. Rojas Delgado, R.M. Jacobberger, S.S. Roy, V.S. Mangu, M.S. Arnold, F. Cavallo, M.G. Lagally, Passivation of germanium by graphene, ACS Appl. Mater. Interfaces 9 (2017) 17629–17636.
[34] P. Braeuninger-Weimer, O. Burton, R.S. Weatherup, R. Wang, P. Dudin, B. Brennan, A.J. Pollard, B.C. Bayer, V.P. Veigang-Radulescu, J.C. Meyer, B. J. Murdoch, P.J. Cumpson, S. Hofmann, Reactive intercalation and oxidation at the buried graphene-germanium interface, Apl. Mater. 7 (2019) 071107.
[35] F. Akhtar, J. Dabrowski, M. Lisker, Y. Yamamoto, A. Mai, C. Wenger, M. Lukosius, Investigation of the oxidation behavior of graphene/Ge(001) versus graphene/Ge (110) systems, ACS Appl. Mater. Interfaces 12 (2020) 3188–3197.
[36] A. Ganguly, S. Sharma, P. Papakonstantinou, J. Hamilton, Probing the thermal deoxygenation of graphene oxide using high-resolution in situ X-ray-based spectroscopies, J. Phys. Chem. C 115 (2011) 17009–17019.
[37] X. Wang, L. Andrews, G.P. Kushto, Infrared spectra of the novel Ge2H2 and Ge2H4 species and the reactive GeH1,2,3 intermediates in solid neon, deuterium and argon, J. Phys. Chem. 106 (2002) 5809–5816.
[38] R. Ludeke, L. Esaki, Electron energy-loss spectroscopy of GaAs and Ge surfaces, Phys. Rev. Lett. 33 (1974) 653–656.
[39] L. Pasquali, S. D'Addato, L. Tagliavini, A.M. Prandini, S. Nannarone, Surface phase transitions of Ge(111)c(2×8) studied by electron energy loss spectroscopy, Surf. Sci. 377–379 (1997) 534–538.
[40] M.K. Kinyanjui, C. Kramberger, T. Pichler, J.C. Meyer, P. Wachsmuth, G. Benner, U. Kaiser, Direct probe of linearly dispersing 2D interband plasmons in a free-standing graphene monolayer, Europhys. Lett. 97 (2012) 57005.
[41] A.V. Generalov, Y.S. Dedkov, EELS study of the epitaxial graphene/Ni(111) and graphene/Au/Ni(111) systems, Carbon 50 (2012) 183–191.
[42] T. Eberlein, U. Bangert, R.R. Nair, R. Jones, M. Gass, A.L. Bleloch, K.S. Novoselov, A. Geim, P.R. Briddon, Plasmon spectroscopy of free-standing graphene films, Phys. Rev. B 77 (2008) 233406.
[43] A. Apponi, D. Convertino, N. Mishra, C. Coletti, M. Iodice, F. Frasconi, F. Pilo, N. S. Blaj, D. Paoloni, I. Rago, G. De Bellis, G. Cavoto, A. Ruocco, Transmission

through graphene of electrons in the 30 – 900 eV range, Carbon 216 (2024) 118502.
[44] J. Lu, K.P. Loh, H. Huang, W. Chen, A.T.S. Wee, Plasmon dispersion on epitaxial graphene studied using high-resolution electron energy-loss spectroscopy, Phys. Rev. B 80 (2009) 113410.
[45] A. Politano, G. Chiarello, Plasmon modes in graphene: status and prospect, Nanoscale 6 (2014) 10927–10940.
[46] A. Politano, I. Radović, D. Borka, Z.L. Mišković, G. Chiarello, Interband plasmons in supported graphene on metal substrates: theory and experiments, Carbon 96 (2016) 91–97.
[47] J. Tesch, E. Voloshina, M. Fonin, Y. Dedkov, Growth and electronic structure of graphene on semiconducting Ge(110), Carbon 122 (2017) 428–433.
[48] Partial coverage of the two domains can be estimated by dividing the Γ-K (Or Γ-M) peak area along one direction by the sum of the Γ-K (Or Γ-M) peaks areas along the φ=0° and φ=30° directions. This calculation reveals that the partial coverage of the larger domain is ≈85%, which is obtained as the average value computed for the Γ-K and Γ-M peaks.
[49] E. Palange, L. Di Gaspare, F. Evangelisti, Real time spectroscopic ellipsometric analysis of Ge film growth on Si(001) substrates, Thin Solid Films 428 (2003) 160–164.
[50] U. Fink, T.A. Wiggins, D.H. Rank, Frequency and intensity measurements on the quadrupole spectrum of molecular hydrogen, J. Mol. Spectrosc. 18 (1965) 384–395.